IJFANS INTERNATIONAL JOURNAL OF FOOD AND NUTRITIONAL SCIENCES
ISSN PRINT 2319 1775 Online 2320 7876
 Journal Volume 10, Iss 08, 2021

HEAT TRANSPORT AND BIO-CONVECTIVE NANOMATERIAL FLOW OF WALTER'S-B FLUID CONTAINING GYROTACTIC MICROORGANISMS

[1]MEERA CHANDRASHEKAR,[2]KIRAN VARAMGANTI
[12]Assistant Professor
Department of Physics
Kshatriya College of Engineering

ABSTRACT:

This research work highlight the newly developed concept of Rosseland approximation and gyrotactic microorganisms in steady, two-dimensional, incompressible flow of Walter's-B nanofluid (non-Newtonian) over a stretchable surface of sheet. Buongiorno nanofluid model, which represents seven important slip mechanisms (i.e., Brownian motion, inertia, Magnus impact, thermophoresis, diffusion-phoresis, gravity and fluid drainage) is utilized in the mathematical modeling of governing expressions. In this research work, only two important factors of seven slip mechanisms (Brownian diffusion, thermophoresis) are studied and the rest of neglected. Furthermore, the Rosseland approximation and heat generation/absorption effects are used in the modeling of the energy equation. The behavior of thermal and solutal stratification effects are addressed at the stretched boundary of the sheet. The nonlinear dimensional flow expressions lead to dimensionless ordinary equations through appropriate similarity transformations. The total residual error is calculated through Homotopy Analysis Method (HAM) for the momentum, temperature, concentration and motile density. The influences of important flow parameters of the governing flow equations are discussed and plotted graphically. The obtained results are compared with fruitful and valuable research in the literature and found very good agreement with them. Over obtained outcomes highlight that the velocity field, declined versus higher estimations of Weissenberg number. It is also remarked that the temperature and concentration fields have contrast impact subject to thermophoresis parameter. The physical quantities like skin friction coefficient, motile density, concentration and Nusselt number are discussed physically via various flow parameters.

Keywords: Walter's-B nanofluid (non-Newtonian fluid) Rosseland approximation Gyrotactic microorganisms Heat generation/absorption Thermophoresis diffusion Brownian motion.

1. Introduction:

Boundary layer flow of non-Newtonian materials play an important role in the modeling of several manufacturing processes in industrial and mechanical engineering. Some of these manufacturing processes comprise adhesive tapes fabrication, plastic sheets aerodynamics, metallic plates, cooling, application of coating and layers onto rigid substrates and so forth others. Some important investigations related to boundary layer flow can be seen in Refs. [1-7]. Refs. [8-15] highlights some significant research work containing non-Newtonian fluids with various flow geometries. In nature, the Walter's-B fluid model is highly nonlinear and it is very difficult to solve. Therefore, numerous researchers and investigators are taking interest in these problems like Chang et al. [16] explore free convective heat transport in the flow of viscoelastic Walter's-B fluid and numerical results are obtained via Finite Difference Method (FDM). Nadeem et al. [17] investigate the magnetized oblique nanomaterial flow of non-Newtonian fluid

(Walter's-B) by a convective stretched surface. Nandeppanavar et al. [18] worked on heat transport and flow of Walter's-B fluid towards an impermeable moving surface with elastic deformation and heat generation/absorption effects. The radiative heat flux and uniform heat generation/absorption effects in fluid low of Walter's-B model with elastic deformation is scrutinized by Hakeem et al. [13]. Hayat et al. [19] discuss the heat transport in fluid flow of Walter's-B fluid, which is magnetized in the presence of applied magnetic field with convective boundary conditions. Hayat et al. [20,21] inspected convective flow of Walter's-B fluid with heat, transportation by a stretched surface by Newtonian heating. Talla [22] deliberated exponentially stretched flow of Walter's-B fluid. Ramesh and Devakar [23] evaluated peristaltic activity in non-Newtonian fluid flow (Walter's-B) in a vertical channel. Hayat et al. [24] depict magnetized and electrical conducting 3D flow of non-Newtonian material with solar radiation.

A nanoliquid is a liquid comprising nanometer-sized particles in a continuous phase liquid, called nanoparticles or metallic particles. The metallic particles utilized in nanoliquids are basically made of carbides or carbon nanotubes, metals and oxides. It is used to increase the thermal conductivity of base liquids. Nanofluids or nanoliquids are numerous applications in several industrial and technological processes, for example wire drawing, melt spinning process, plastic film production, fiberglass and so many others. The effective transportation of heat frequently depends on material type, shape of particles and number of submerged nanoparticles. Furthermore, nanoliquids have used formation and structural process of power generators, petroleum reservoirs, nuclear reactors cooling, vehicle transformer, and fiber production in textile, geothermal energy, cancer therapy and safer surgery processes. Initially, Choi and Eastman [25] was experimentally discussed the features of nanoparticles in a continuous phase fluid and their obtained outcomes reveal that the thermal conductivity of base fluid more increase by the insertion of metallic particles. After Choi and Eastman, Buongiorno [26] revealed that heat efficiency of conventional working materials is improved through Brownian motion and thermophoresis diffusion. Hayat el al. [27] worked on irreversibility analysis in second grade fluid flow submerged in a base fluid with thermal radiation. Refs. [28-30] illustrates the behavior of nanofluid flow towards stretched surfaces.

The bio-convection phenomenon arises due to average upward swimming of microorganisms (which are denser then water). Upward swimming of microorganisms tends to concentrate on the upper portion of the fluid layer, causing a top heavy density stratification that often becomes unstable. Bio-convection describes density stratification and spontaneous pattern formation induced by nanoparticles and buoyancy forces and simultaneous interaction of the denser self-propelled microorganisms. When gyrotactic microorganisms are added into a nanofluid stability of nanofluid upsurges. Due to gravity, light and chemical reactions motile microorganisms swim in the upward direction. Adding motile microorganisms to the suspensions have contributed to the bio micro-systems such as enzyme biosensor and micro fluidics devices such as bacteria powered micro mixers especially in micro- volumes. Tham et al. [31] scrutinized nanofluid flow having gyrotactic microorganisms and mixed convection moving towards a solid sphere embedded in a porous medium. Aziz et al. [32] considered nanoliquid free convective flow having motile microorganisms. Xu and Pop [33] evaluated mixed bio-convective flow filled in a horizontal channel and fully developed containing gyrotactic microorganisms and nanoparticles. Kuznetsov [34] examined bio-convection due to gyrotactic microorganisms and nanofluid particle. In the next, Kuznetsov [35] considered nanofluid bio-thermal convection considering effects of Oxytactic microorganisms and gyrotactic microorganisms. Khan et al. [36] recently

deliberated free convective flow of non-Newtonian fluids having nanoparticles and gyrotactic microorganisms embedded in a porous medium. Tausif et al. [37] discussed bio-convective flow of a nanofluid containing nanoparticles and gyrotactic microorganisms with multiple slip effects. Siddiqa et al. [38] studied the flow of nanofluid past a vertical wavy surface with gyrotactic bio-convection. Mutuku and Makinde [39] considered hydro-magnetic bio-convective nanofluid flow over a permeable vertical plate with gyrotactic microorganisms. Makinde and Animasaun [40] examined MHD bio-convective flow of a nanofluid past an upper surface of revolution of a paraboloid with thermal radiation and chemical reaction. Raees et al. [41] analyzed 3D stagnation point flow of nanofluid on a moving surface having isotropic slip containing both microorganisms and nanoparticles. Akbar and Khan [42] studied nanofluid flow with magnetic field and suspen sion of gyrotactic microorganisms. Raju and Sandeep [43] examined MHD non-Newtonian bio-convective flow in rotating cone/plate with cross diffusion. Hoecker-Martínez and Smyth [44] studied gyrotactic organisms trapping in unstable shear layers.

The prime aim of this research letter is to explore the concept of Rosseland approximation and gyrotactic microorganisms in steady, two-dimensional, incompressible flow of Walter's-B nanofluid (non-Newtonian) over a stretchable surface of the sheet. Buongiorno nanofluid model, which represents seven important slip mechanisms (i.e., Brownian motion, inertia, Magnus impact, thermophoresis, diffusion-phoresis, gravity and fluid drainage) is utilized in the mathematical modeling of governing expressions. In this research work, only two important factors of seven slip mechanisms (Brownian diffusion, thermophoresis) are studied and the rest of neglected. Furthermore, the Rosseland approximation and heat generation/absorption effects are used in the modeling of the energy equation. The behavior of thermal and solutal stratification effects are addressed at the stretched boundary of the sheet. The nonlinear dimensional flow expressions lead to dimensionless ordinary equations through appropriate similarity transformations. The total residual error is calculated through Homotopy Analysis Method (HAM) [8,45-53] for the momentum, temperature, concentration and motile density.

2. Modeling

Here, the newly developed concept of Rosseland approximation and gyrotactic microorganisms in two-dimensional, steady, incompressible non-magnetized flow of Walter's-B fluid is addressed towards a stretched surface. The flow is nonlinear and generated by stretching phenomenon. The energy equation is based on the first law of thermodynamics and modeled in the presence of radiative heat flux and heat generation/absorption. Furthermore, concentration and motile density is discussed. Both thermal and solutal stratification conditions are imposed at the boundary of the stretched surface, which comprising of fluid parcels of various densities. Flow diagram is presented in Fig. 1.Fig. 2a.Fig. 2b.

Let $u = U_w(x) = ax$ highlights the stretching velocity of the sheet. The governing partial differential equations are considered flow problem are listed as

$$\frac{\partial u}{\partial x} + \frac{\partial v}{\partial y} = 0, \tag{1}$$

$$u\frac{\partial u}{\partial x} + v\frac{\partial u}{\partial y} = \frac{\mu_0}{\rho}\frac{\partial^2 u}{\partial y^2} - \frac{k_0}{\rho}\left(u\frac{\partial^3 u}{\partial x \partial y^2} + v\frac{\partial^3 u}{\partial y^3} - \frac{\partial u}{\partial y}\frac{\partial^2 u}{\partial x \partial y} + \frac{\partial u}{\partial x}\frac{\partial^2 u}{\partial y^2}\right), \tag{2}$$

$$u\frac{\partial T}{\partial x} + v\frac{\partial T}{\partial y} = \frac{k}{(\rho c_p)_f}\left(\frac{\partial^2 T}{\partial y^2}\right) + \tau D_B\left(\frac{\partial C}{\partial y}\frac{\partial T}{\partial y}\right) + \frac{\tau D_T}{T_\infty}\left(\frac{\partial T}{\partial y}\right)^2 - \frac{1}{(\rho c_p)_f}\frac{\partial q_r}{\partial y} + \frac{Q_0}{(\rho c_p)_f}(T - T_\infty), \tag{3}$$

$$u\frac{\partial C}{\partial x} + v\frac{\partial C}{\partial y} = D_B\frac{\partial^2 C}{\partial y^2} + \frac{D_T}{T_\infty}\frac{\partial^2 T}{\partial y^2}, \tag{4}$$

$$u\frac{\partial N}{\partial x} + v\frac{\partial N}{\partial y} + \frac{bW_c}{(C_w - C_0)}\left[\frac{\partial}{\partial y}\left(N\frac{\partial C}{\partial y}\right)\right] = D_m\frac{\partial^2 N}{\partial y^2}, \tag{5}$$

ISSN PRINT 2319 1775 Online 2320 7876
 Journal Volume 10, Iss 08, 2021

$$u = U_w(x) = ax,\ v = 0,\ T = T_w = T_0 + Ax,\ C = C_w = C_0 + Bx,\ N =$$
$$u \to 0,\ T \to T_\infty = T_0 + Ex,\ C \to C_\infty = C_0 + Fx,\ N \to N_\infty =$$

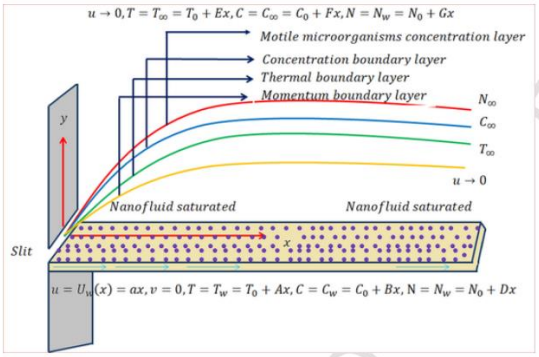

Fig. 1. Schematic flow diagram

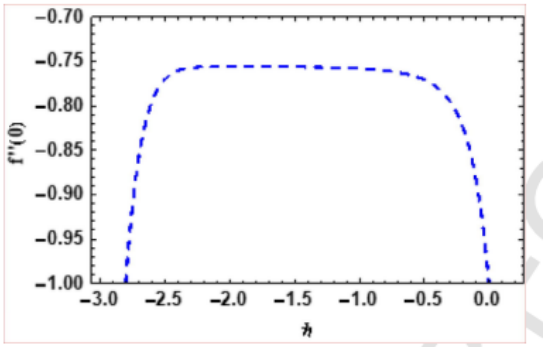

Fig. 2a. $h-curveforf''(0)$.

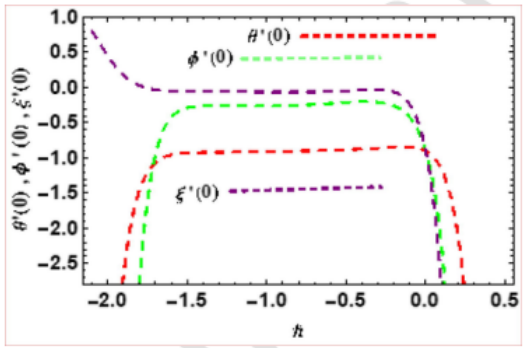

Fig. 2b. $h-curveforθ'(0), \phi'(0)\ and \xi'(0)$.

Note that, x,y signifies the Cartesian coordinates, density, velocity components, short memory coefficient, viscosity, temperature, thermal conductivity, specific heat, ratio of heat $\tau\left(=\frac{(\rho c_p)_p}{(\rho c_p)_f}\right)$ capacities, Brownian motion, concentration, thermophoretic diffusion, coefficient of radiative heat flux, coefficient of heat generation/absorption, ambient temperature, concentration of microorganisms, ambient concentration, chemotaxis constant, microorganisms diffusion coefficient, maximum cell swimming velocity, stretching velocity, dimensional constant, wall temperature, dimensional constant, reference temperature, concentration, motile microorganisms and ambient motile density of microorganisms. The radiative heat flux in the presence Rosseland approximation is defined as mophoretic diffusion, coefficient of radiative heat flux, coefficient of heat generation/absorption, ambient temperature, concentration of microorganisms, ambient concentration, chemotaxis constant, microorganisms diffusion coefficient, maximum cell swimming velocity, stretching velocity, dimensional constant, wall temperature, dimensional constant, reference temperature, concentration, motile microorganisms and ambient motile density of microorganisms.

The radiative heat flux in the presence Rosseland approximation is defined as

$$q_r = -\frac{4\sigma^*}{k^*}\frac{\partial T^4}{\partial y} = -\frac{16\sigma^*}{3k^*}\frac{\partial T}{\partial y}, \tag{7}$$

where signifies the Stefan-Boltzman constant and and mean absorption coefficient.

Letting

$$\left.\begin{aligned} u = axf'(\eta),\ v = -\sqrt{av}f(\eta),\ \eta = \sqrt{\tfrac{a}{v}}y, \\ \theta(\eta) = \tfrac{T-T_\infty}{T_w-T_0},\ \phi(\eta) = \tfrac{C-C_\infty}{C_w-C_0},\ \xi(\eta) = \tfrac{N-N_\infty}{N_w-N_0}. \end{aligned}\right\} \tag{8}$$

We arrive

$$f''' + ff'' - f'^2 + \beta[f''^2 - 2f'f''' + ff^{(iv)}] = 0, \tag{9}$$

$$\theta'' + \tfrac{4}{3}R\left[3\delta\theta^2 + 3\delta^3\theta^2\theta^2 + 6\delta^2\theta\theta^2 + \theta'' + \delta^3\theta^3\theta'' + 3\delta^2\theta^2\theta'' + 3\delta\theta\theta''\right] - PrS_1 f' - Prf'\theta + Prf\theta' + Pr\delta_1\theta + PrNb\theta'\phi' + PrNt\theta'^2 = 0, \tag{10}$$

$$\phi'' + \frac{Nt}{Nb}\theta'' + Scf\phi' - Scf'\phi - ScS_2 f' = 0, \tag{11}$$

$$\xi'' - LbS_3 f' - Lbf'\xi + Lbf\xi' - Pe\left[\phi'\xi' + \Omega\phi'' + \xi\phi''\right], \tag{12}$$

$$f(0) = 0,\ f'(0) = 1,\ \theta(0) = 1 - S_1,\ \phi(0) = 1 - S_2,\ \text{and}\ \xi(0) = 1 - S$$
$$f'(\infty) \to 0,\ \theta(\infty) \to 0,\ \phi(\infty) \to 0,\ \text{and}\ \xi(\infty) \to 0.$$

ISSN PRINT 2319 1775 Online 2320 7876
 Journal Volume 10, Iss 08, 2021

where $\beta\left(=\frac{ak_0}{\mu_0}\right)$ highlights the Weissenberg number, $R\left(=\frac{4\sigma^* T_\infty^3}{3k^* k}\right)$ thermal radiation parameter, $\delta=\left(\frac{T_w-T_\infty}{T_\infty}\right)$ temperature ratio parameter,

$\Pr\left(=\frac{\mu_0 c_p}{k}\right)$ Prandtl number, $S_1\left(=\frac{E}{A}\right)$ thermal stratification parameter, $\delta_1\left(=\frac{Q_0}{(\rho c_p)_f a}\right)$ heat generation absorption parameter, $Nb\left(=\frac{(\rho c_p)_s D_B(C_w-C_0)}{(\rho c_p)_f \nu}\right)$ Brownian motion parameter, $S_2\left(=\frac{F}{B}\right)$ concentration stratification parameter, $Nt\left(=\frac{(\rho c_p)_s D_T(T_w-T_0)}{(\rho c_p)_f \nu T_\infty}\right)$ thermophoretic parameter, $Sc\left(=\frac{\nu}{D_B}\right)$ Schmidt number, $Lb\left(=\frac{\nu}{D_m}\right)$ Bio-convection Lewis number, $\Omega\left(=\frac{N_\infty}{N_w-N_0}\right)$ microorganisms concentration difference parameter, $Pe\left(=\frac{bW_c}{D_m}\right)$ Bio-convection Peclet number and $S_3\left(=\frac{G}{D}\right)$ motile density stratification parameter.

3. Physical interest

In mathematical point of view, the skin friction coefficient, local density number, heat transfer rate and gradient of concentration are communicated as

$$\left.\begin{aligned} C_{fx}=\frac{2\tau_w}{\rho U_w^2},\ Nu_x=-\frac{xq_w}{k(T_w-T_0)},\\ Sh_x=\frac{xq_m}{D_B(C_w-C_0)} \text{ and } Nn_x=\frac{xq_n}{D_n(N_w-N_0)}. \end{aligned}\right\} \quad (14)$$

where and are addressed as

$$\left.\begin{aligned} \tau_w=\mu_0\left(\frac{\partial u}{\partial y}\right)_{y=0}-k_0\left(u\frac{\partial^2 u}{\partial x\partial y}-2\frac{\partial u}{\partial x}\frac{\partial u}{\partial y}\right),\ q_m=-D_B\left(\frac{\partial C}{\partial y}\right)_{y=0}\\ q_w=-k_f\left(1+\frac{16\sigma^* T^3}{3k^* k_f}\right)\left(\frac{\partial T}{\partial y}\right)_{y=0},\ q_n=-D_n\left(\frac{\partial N}{\partial y}\right)_{y=0}. \end{aligned}\right\} \quad (15)$$

The dimensionless form is

$$\left.\begin{aligned} \frac{1}{2}C_{fx}Re_x^{0.5}=f''(0)\left[1+\beta f'(0)\right],\\ Nu_x Re_x^{-0.5}=-\left[1+\frac{4}{3}R(1+\delta\theta(0))^3\right]\theta'(0),\\ Sh_x Re_x^{-0.5}=-\phi'(0),\ Nn_x Re_x^{-0.5}=-\xi'(0), \end{aligned}\right\} \quad (16)$$

where signifies the local Reynold number.

4. Methodology

Here HAM is implemented to get the series solution of governing equations. The initial guesses and linear operators are communicated as

$$\left.\begin{aligned} f_0(\eta)=1-e^{-\eta},\ \theta_0(\eta)=(1-S_1)\,e^{-\eta},\\ \phi_0(\eta)=(1-S_2)\,e^{-\eta},\ \xi_0(\eta)=(1-S_3)\,e^{-\eta}, \end{aligned}\right\} \quad (17)$$

$$\left.\begin{aligned} \Im_f=f'''-f',\ \Im_\theta=\theta''-\theta\\ \Im_\phi=\phi''-\phi,\ \Im_\xi=\xi''-\xi, \end{aligned}\right\} \quad (18)$$

which satisfies the characteristics

$$\left.\begin{aligned} \Im_f\left(c_1+c_2e^{\eta}+c_3e^{-\eta}\right)=0,\ \Im_\theta\left(c_4e^{\eta}+c_5e^{-\eta}\right)=0,\\ \Im_\phi\left(c_6e^{\eta}+c_7e^{-\eta}\right)=0,\ \Im_\xi\left(c_8e^{\eta}+c_9e^{-\eta}\right)=0, \end{aligned}\right\} \quad (19)$$

where $c_i\,(i=1-9)$ indicates arbitrary constants

5. Convergence analysis

In homotopy approach auxiliary variables i.e., and control and regulate region of convergence of series solution. In Fig. 2a and Fig. 2b we have plotted the curves for velocity, temperature, concentration and motile density profiles.

The suitable ranges of auxiliary variables i.e., $\hbar_f$, $\hbar_\theta$, $\hbar_\phi$ and $\hbar_\xi$ are

$$-2.8\leqslant\hbar_f\leqslant 0.1,\ -2.0\leqslant\hbar_\theta\leqslant 0.2,\ -1.8\leqslant\hbar_\phi\leqslant 0.2,\ -1.6\leqslant\hbar_\xi\leqslant 0.1.$$

The convergence of obtained solutions is also justified numerically in Table 1. From Table 1, it is noticed that 20th order of iterations are sufficient for $f''(0)$ and $\xi'(0)$ and 25th order of iterations are sufficient for $\theta'(0)$ and $\phi'(0)$. Table 2 represents the comparative investigation of present work with Saleem el al. [54] and noticed a very good agreement with them.

Table 1
Various numerical iterations for $f''(0)$, $\theta'(0)$, $\phi'(0)$ and $\xi'(0)$.

Iterations	$-f''(0)$	$-\theta'(0)$	$-\phi'(0)$	$-\xi'(0)$
1	0.866	0.799	0.260	−0.022
5	0.772	0.878	0.189	0.038
10	0.759	0.903	0.257	0.064
15	0.757	0.916	0.258	0.058
20	0.756	0.926	0.261	0.060
25	0.756	0.927	0.264	0.060
30	0.756	0.927	0.264	0.060

6. Discussion

Salient characteristics of pertinent flow parameters on the $(f'(\eta))$, $(\theta(\eta))$, $(\phi(\eta))$ and $(\xi(\eta))$ are analyzed in this section, where indicates the velocity field, $\theta(\eta)$highlights the temperature, $(\phi(\eta))$ signifies the concentration and denotes the motile density.

6.1. Velocity field

Impact of Weissenberg number on the velocity field is displayed in Fig. 3. Physically, Weissenberg number is the ratio of short memory coefficient and viscosity. Here, velocity field declines versus higher values of Weissenberg number. In physical point of view, short memory coefficient boosts up in the presence of larger Weissenberg number, which enhance the velocity field. Also, the boundary layer decays against larger Weissenberg number.

Table 2
Comparative examination of present work with Saleem el al. [54] in special case.

Pr	Sc	Saleem et al. [54]		Present results	
Pr	Sc	Skin friction	Nusselt number	Skin friction	Nusselt number
0.7	0.22	1.55443	0.92494	1.55440	0.92424
	0.60	1.39259	0.90199	1.39251	0.90198
	0.94	1.31339	0.86679	1.31331	0.86672
3.0	0.22	1.28595	1.79670	1.28590	1.79669
	0.60	1.12921	1.76650	1.12920	1.76648
	0.94	1.05230	1.75182	1.05229	1.75181

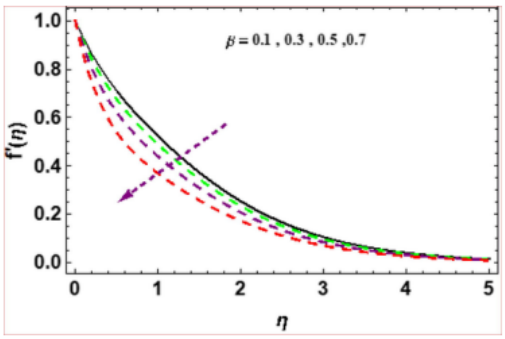

Fig. 3. $f'(\eta)$ versus β.

6.2. Temperature distribution

Figs. $(4-10)$ are plotted to examine the salient characteristics of Nb, and $\Pr, S_1$ and R on $(\theta(\eta))$. Fig. 4 is outlined to show the influence of Nb on $(\theta(\eta))$ It is observed $(\theta(\eta))$ that is increased via larger values of Brownian motion parameter. Also, the boundary layer thickness boosts by higher estimations of Brownian motion parameter. The influence of Prandtl number on $(\theta(\eta))$ is sketched in Fig. 5. As anticipated, both thermal field and associated layer diminishes subject to rising values of Prandtl number. Mathematically, Prandtl number is the ratio of momentum diffusivity to heat diffusivity. In heat transport fluid problems, it controls the relative thickness of thermal as well as the momentum boundary layers. If Pr is small, it tells us that thermal diffusion is more in comparison to momentum diffusion. That is for a present flow problem, the flow conditions remaining the same, if we want larger heat transport rate we have to utilize a liquid that has smaller Pr Fig. 6 discloses the salient characteristics of thermal stratified variable on temperature profile. Clearly, it is remarked that both thermal field and layer thickness are declined versus higher values of thermal stratified variable. Physically, the effective convective potential that occurs between the ambient nanofluid and nonlinear stretching sheet diminished subject to rising values of thermal stratified variable. Therefore, the thermal layer thickness and material temperature declined for rising thermal stratified parameter. Fig. 7 displayed the behavior of radiation parameter on $(\theta(\eta))$.As anticipated, both fluid temperature and its associated layer thickness are increasing function of radiation parameter. An enhancement in radiation parameter boosts the heat flux from the heated stretched surface and consequently upsurges the fluid temperature.

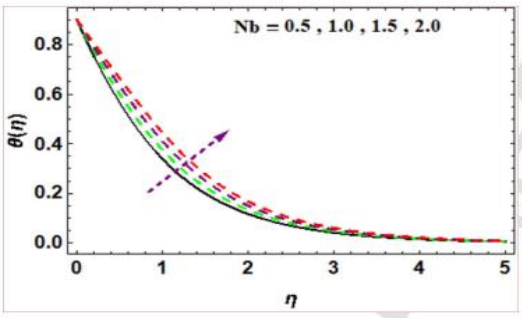

Fig. 4. $\theta(\eta)$ versus Nb.

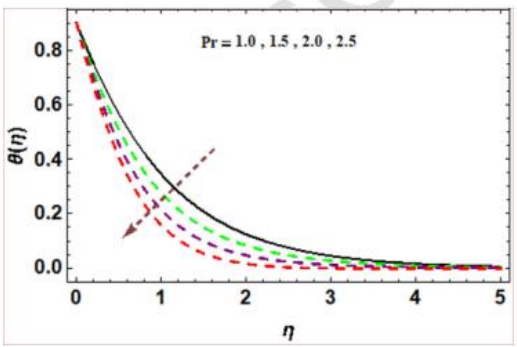

Fig. 5. $\theta(\eta)$ versus Pr.

ISSN PRINT 2319 1775 Online 2320 7876
 Journal Volume 10, Iss 08, 2021

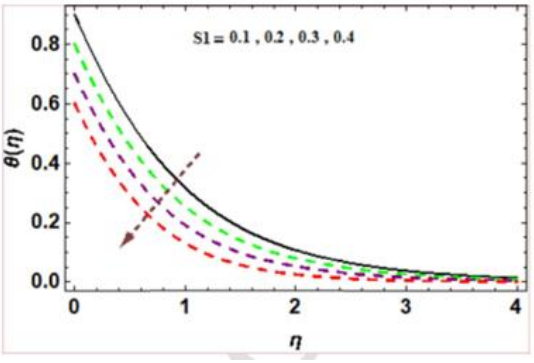

Fig. 6. $\theta(\eta)$ versus S_1.

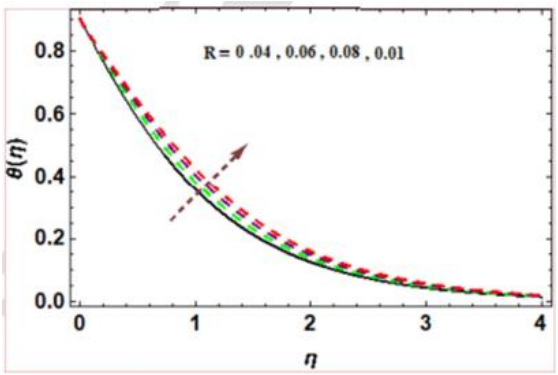

Fig. 7. $\theta(\eta)$ versus R.

6.3 Concentration field

Figs. 8-10 are developed to discuss the concentration field versus thermophoresis parameter, solutal stratified parameter and Schmidt number. The influence of Nt on $(\phi(\eta))$ is demonstrated in Fig. 8. Clearly, it is remarked that the nanomaterial concentration boosts up subject to larger thermophoretic parameter. Physically, it is due to the thermophoretic force created by rate of mass transport at the stretchable surface generates a smooth flow far from the stretching surface. More heated liquid shift away from the stretched surface and as a result larger amount of Nt .The fast flow from the stretching surface via thermophoretic force resulting to upsurge in the concentration layer thickness. Figs. 9 and 10 are plotted to check to how solutal stratified parameter and Schmidt number affect the nanoparticle concentration.

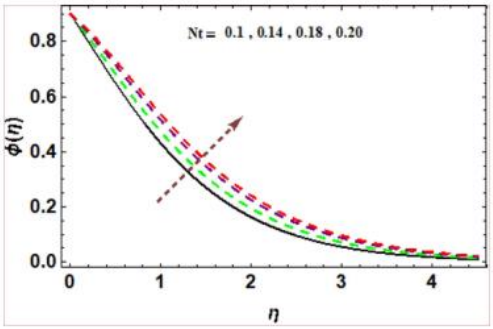

Fig. 8. $\phi(\eta)$ versus Nt.

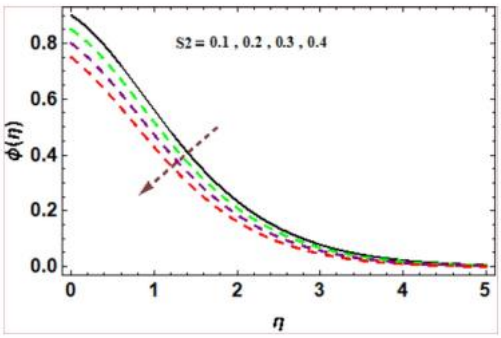

Fig. 9. $\phi(\eta)$ versus S_2.

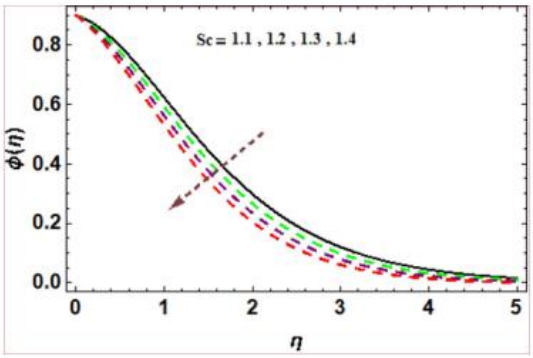

Fig. 10. $\phi(\eta)$ versus Sc.

field. Clearly, for higher estimations of solutal stratified parameter and Schmidt number, the nanoparticle concentration decreases. The ratio of kinematic viscosity to molecular diffusion coefficient $\left(Sc = \frac{\nu}{D_B}\right)$ is called the Schmidt number. Here, mass diffusivity decays against rising Schmidt number which reduces the nanomaterial concentration.

6.3. Motile density

Figs.(11-13) are organized to analyze the influence of Bio-convection Lewis number Lb, Peclet number Pe, and motile density stratified parameter on Fig. 11 displays the salient

influence of on Here, shows decreasing behavior on Furthermore, motility layer declines versus larger The variation in liquid motility subject to positive estimations of and is discussed in Figs. 12.

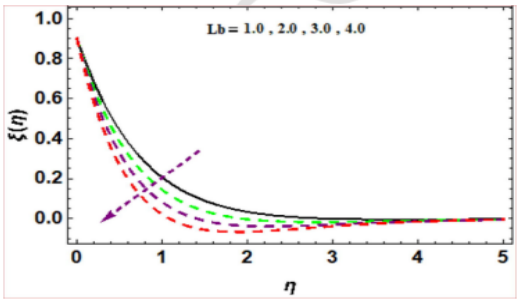

Fig. 11. $\xi.(\eta)$ versusLb.

and 13. For growing values of s3 and Pe the fluid motility distribution declines. It is also noticed from this figures that motility layer also diminishes against larger Peclet number and motile density stratified parameter.

6.4. Physical interest

The physical quantities like, skin friction coefficient $(C_{fx}Re_x^{0.5})$ Nusselt number $(Nu_xRe_x^{-0.5})$ Sherwood number $(Sh_xRe_x^{-0.5})$ and local density number $(Nn_xRe_x^{-0.5})$ are discussed graphically versus pertinent flow parameters i.e., , β, δ, R, Nb, Nt, Ω and Pe. Physical behavior of $(C_{fx}Re_x^{0.5})$ against rising values of and is portrayed in Fig. 14. As predicted, the magnitude of drag force boosts up against increasing behavior of Weissenberg number. Impact of heat transfer rate against and is depicted in Fig. 15. Here same behavior like skin

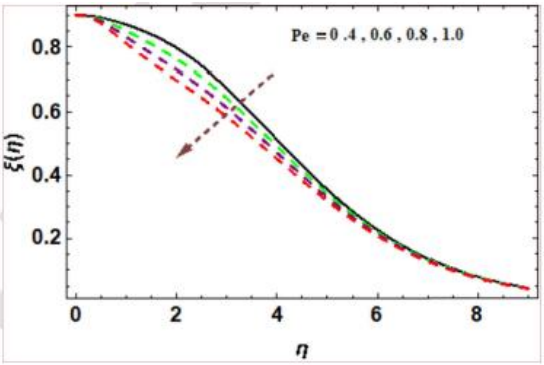

Fig. 12. $\xi.(\eta)$ versusPe.

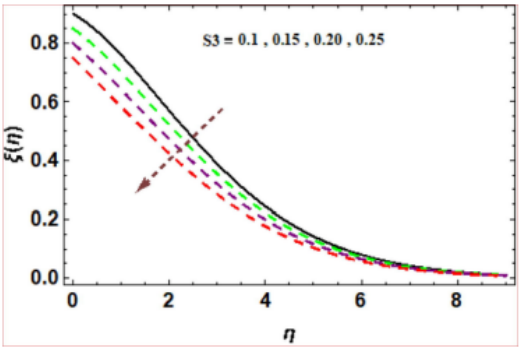

Fig. 13. $\xi.(\eta)$ versusS_3.

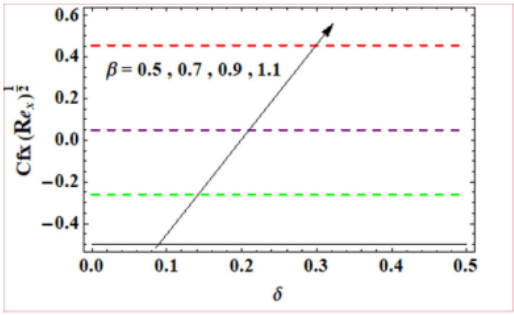

Fig. 14. *Skinfrictionversusδandβ.*

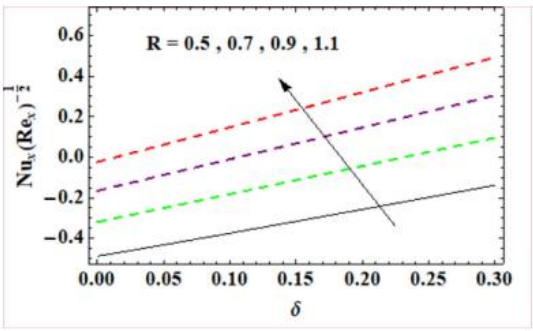

Fig. 15. *NusseltnumberversusRandδ.*

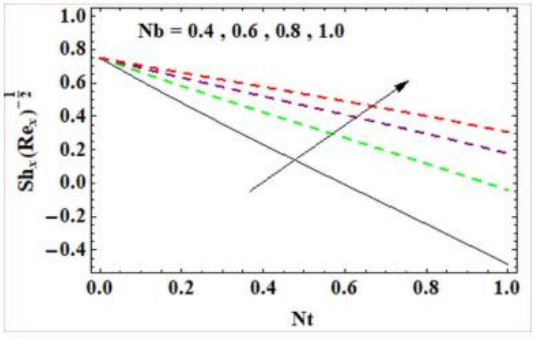

Fig. 16. *SherwoodnumberversusNbandNt.*

friction is observed for growing values of radiation parameter and Fig. 16 is drawn for

the impact of Brownian motion and thermophoretic parameter on the Sherwood number. As anticipated, the behavior of Sherwood number boosts versus larger Brownian motion variable and thermophoretic parameter. Fig. 17 is sketched to examine how Lb and Pe affect the $(Nn_xRe_x^{-0.5})$. Clearly, the behavior of $(Nn_xRe_x^{-0.5})$ declines subject to higher estimations of Lb and pe.

7. Conclusions

The prime objective of this research communication is to explore the concept of gyrotactic microorganisms and Rosseland approximation in fully radiated steady, two-dimensional, incompressible flow of Walter's-B nanofluid (non-Newtonian) towards a stretched surface. Mathematically modeling is performed through implementation of Buongiorno nanofluid model, which represents seven important slip mechanisms (i.e., Brownian motion, inertia, Magnus impact, thermophoresis, diffusion-phoresis, gravity and fluid drainage). In this research work, only two important factors of seven slip mechanisms (Brownian diffusion, thermophoresis) are studied and the rest of neglected. The desired governing equations are solved through homotopy analysis method. The prime and main outcomes are listed as

The velocity of fluid is less by increasing the values of Weissenberg number.

• Thermal field and associated layer thickness boosts up against larger Brownian motion parameter.

• Nanomaterial concentration is more subject to thermophoretic parameter.

• Motility profile and motility layer thickness been decreased versus motile density stratified parameter.

• The impact of skin friction coefficient decreases by increasing Weissenberg number. • Heat and mass transfer rates have similar behavior versus radiation parameter and Brownian motion parameter respectively.

• Motile density rate diminishes subject to Bio-convection Lewis number and Peclet number.

References:

[1] K.L. Hsiao Heat and mass transfer for micropolar flow with radiation effect past a nonlinearly stretching sheet. Heat and Mass Transf. 2010;46:413–419.

[2] T. Hayat, M.I. Khan, M. Farooq, A. Alsaedi, M. Waqas, T. Yasmeen Impact of Cattaneo-Christov heat flux model in flow of variable thermal conductivity fluid over a variable thicked surface. Int. J. Heat Mass Transf. 2016;99:702–710.

[3] U. Adnan, N. Ahmed Khan, S.T. Mohyud-Din Thermo-diffusion and diffusion-thermo effects on flow of second grade fluid between two inclined plane walls. J. Mol. Liq. 2016;224:1074–1082.

[4] M.I. Khan, M. Waqas, T. Hayat, A. Alsaedi A comparative study of Casson fluid with homogeneous-heterogeneous reactions. J. Colloid Interface Sci. 2017;498:85–90.

[5] S.Z.A. Adnan, U. Zaidi, N. Khan, S.T. Ahmed, Yu-Ming Chu Mohyud-Din, I. Khan, et al. Impacts of freezing temperature based thermal conductivity on the heat transfer gradient in nanofluids: applications for a curved Riga surface. Molecules 2020;25:2152.

[6] M.I. Khan, F. Alzahrani, A. Hobiny, Z. Ali Fully developed second order velocity slip Darcy-Forchheimer flow by a variable thicked surface of disk with entropy generation. Int. Commu. Heat Mass Transf. 2020;117:104778.

[7] M. Adnan, U. Asadullah, N. Ahmed Khan, S.T. Mohyud-Din Analytical and numerical investigation of thermal radiation effects on flow of viscous incompressible fluid with stretchable convergent/divergent channels. J. Mol. Liq. 2016;224:768–775.

[8] M.I. Khan, F. Alzahrani, A. Hobiny Heat transport and nonlinear mixed convective nanomaterial slip flow of Walter-B fluid

containing gyrotactic microorganisms. Alex. Eng. J. 2020;59:1761–1769.

[9] A. Hussain, A. Ullah Boundary layer flow of a Walter's B fluid due to a stretching cylinder with temperature dependent viscosity. Alex. Eng. J. 2016;55:3073–3080.

[10] M. Javed, T. Hayat, M. Mustafa, B. Ahmad Velocity and thermal slip effects on peristaltic motion of Walters-B fluid. Int. J. Heat Mass Transf. 2016;96:210–217.

[11] S. Nadeem, N.S. Akbar Influence of heat and chemical reactions on Walter's B fluid model for blood flow through a tapered artery. J. Taiwan Instit. Chem. Eng. 2011;42:67–75. [12] M.M. Nandeppanavar, M.S. Abel, J. Tawade Heat transfer in a Walter's liquid B fluid over an impermeable stretching sheet with non-uniform heat source/sink and elastic deformation. Commu. Nonlinear Sci. Numer. Simul. 2010;15:1791–1802.

[13] A.K.A. Hakeem, N.V. Ganesh, B. Ganga Effect of heat radiation in a Walter's liquid B fluid over a stretching sheet with non-uniform heat source/sink and elastic deformation. J. King Saud Uni.-Eng. Sci. 2014;26:168–175.

[14] R. Naz, S. Tariq, H. Alsulami Inquiry of entropy generation in stratified Walters' B nanofluid with swimming gyrotactic microorganisms. Alex. Eng. J. 2020;59:247–261.

[15] M.I. Khan, M. Waqas, T. Hayat, A. Alsaedi, M.I. Khan Significance of nonlinear radiation in mixed convection flow of magneto Walter-B nanoliquid. Int. J. Hydrogen Energy 2017;42:26408–26416.

[16] T.B. Chang, A. Mehmood, O.A. Beg, M. Narahari, M.N. Islam, F. Ameen Numerical study of transient free convective mass transfer in a Walters-B viscoelastic flow with wall suction. Commu. Nonlinear Sci. Numer. Simul. 2011;16:216–225.

[17] S. Nadeem, R. Mehmood, S.S. Motsa Numerical investigation on MHD oblique flow of Walter's B type nanofluid over a convective surface. Int. J. Thermal Sci. 2015;92:162–172. [18] M.M. Nandepanavar, M.S. Abel, J.V. Tawade Heat transfer in aWalter's liquid B fluid over an impermeable stretching sheet with non-uniform heat source/sink and elastic deformation. Commu. Nonlinear Sci. Numer. Simul. 2010;15:1791–1802.

[19] T. Hayat, S. Asad, M. Mustafa, H.H. Alsulami Heat transfer analysis in the flow of Walters' B fluid with a convective boundary condition. Chin. Phys. B 2014;23:084701.

[20] T. Hayat, A. Shafiq, M. Mustafa, A. Alsaedi Boundary-layer flow of Walters' B fluid with Newtonian heating. Zeitschrift fur Naturforschung A 2015;70:333–341.

[21] H. Talla Numerical study of flow of Walter's liquid B over an exponentially stretching sheet. Int. J. Sci. Resear. Pub. 2013;3:2250–3153.

[22] S.A. Madani, R. Akbar, R. Khoeilar On the study of viscoelastic Walter's B fluid in boundary layer flows. Math. Prob. Eng. 2012;2012:861508.

[23] K. Ramesh, M. Devakar Effect of heat transfer on the peristaltic flow of Walter-B fluid in a vertical channel with external magnetic field. J. Aerospace Eng. 2015;10:04015050. [24] T. Hayat, M. Awais, S. Asghar Radiative effects in a three-dimensional flow of MHD Eyring-Powell fluid. J. Egyp. Math. Soc. 2013;21:379–384.

[25] S.U.S. Choi, J.A. Eastman Enhancing thermal conductivity of fluids with nanoparticles. ASME Publications-Fed 1995;231:99–106.